Gazi University Journal of Science
GU J Sci
26(3):501-508 (2013)

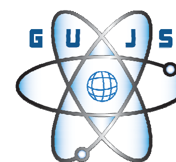

Dielectric Permittivity, AC Conductivity and Electric Modulus Properties of Metal/Ferroelectric/Semiconductor (MFS) Structures

Adem TATAROĞLU[1,♠]

[1]*Physics Department, Faculty of Arts and Sciences, Gazi University, 06500, Teknikokullar, Ankara, TURKEY*

Received:03/07/2013 Accepted:15/07/2013

Abstract

Metal-ferroelectric-semiconductor (MFS) structures were established on n-Si by using $Bi_4Ti_3O_{12}$, a ferroelectric material. Dielectric permittivity, conductivity and modulus properties of MFS structure were characterized through capacitance-voltage (C-V) and conductance-voltage (G/ω-V) measurements. Frequency and temperature dependence of these properties were studied in the ranges of 1 kHz-1 MHz and 100-400 K, respectively. It is observed that the C and G/ω values decrease with the increasing frequency, while they increase with the increasing temperature. The values of the ε' and ε'' are found to decrease with the increasing frequency and increase with the increasing temperature. The σ_{ac} is found to increase with the increasing frequency and temperature. In addition, the real (M') and imaginary (M'') components of the electrical modulus were calculated from the values of ε' and ε''. Activation energy (E_a), from the Arrhenius plot, is also studied to discuss the conduction mechanism in MFS structure.

Keywords: MFS structures; C-V and G/ω-V measurements; dielectric permittivity; ac conductivity; electric modulus

1. INTRODUCTION

Ferroelectrics are a special group of advanced electronic materials consisting of dielectrics which are spontaneously polarized and possess the ability to switch their internal polarization with an applied electric field. Ferroelectric thin films have additional advantages such as lower operating voltage, higher speed and unique sub-micro level structure. Because of these properties ferroelectric thin films are used in applications in the area of dielectric barrier layers and random access memories [1,2]. Memory devices using ferroelectric material may be categorized in to ferroelectric random access memory (FRAM) and dynamic random access memory (DRAM), and metal-ferroelectric-semiconductor field effect transistors (MFS-FETs) [3,4].

MFS-FET, in which, a spontaneous polarization of ferroelectric films is used as a gate insulator, have the potential advantages of high switching speed, nonvolatile data storage, radiation tolerance and high density [5-7]. For this type of structure, it is necessary to form ferroelectric films directly on semiconductor substrate. There is immense potential for many new functional devices to be made by combining ferroelectric materials and semiconductors. By directly interfacing a ferroelectric with a semiconducting material, it is possible to construct several types of interesting field effect devices in which basic electrical properties of the semiconductor can be modified by the polarization state of the adjacent ferroelectric [8].

Metal-ferroelectric-semiconductor (MFS) structured nonvolatile memories have been extensively investigated [7-11]. One of the drawbacks of the MFS-structured memories is the diffusion of the constituent elements of ferroelectrics into the Si substrates. The MFS has been used as a structure for ferroelectric field effect transistor (FET)-type nonvolatile memories [9-

♠Corresponding author, e-mail: ademt@gazi.edu.tr

11]. MFS structure has many problems such as difficulty in depositing ferroelectric thin films directly on silicon, high trap densities, and diffusion of elements into silicon. A possible solution of these problems is to use an insulator buffer layer such as SiO_2, TiO_2, and SnO_2 between the ferroelectric and silicon [12].

Bismuth titanate ($Bi_4Ti_3O_{12}$) with high dielectric constant, a well-known ferroelectric material, is a member of the family of layer-type compounds. It is a good candidate for high-temperature piezoelectric applications, memory storage capacitors, optical memories and electro-optic devices [13-17]. $Bi_4Ti_3O_{12}$ (BTO) films generally have low coercive field, high dielectric constant, high breakdown strength and peculiar switching behavior [18]. A number of methods have been successfully developed to prepare ferroelectric BTO thin films, including physical methods such as rf sputtering, pulsed laser deposition, and chemical methods such as chemical vapor deposition, metal-organic decomposition and sol-gel process [14,19-21]. However, this ferroelectric material layer at metal-semiconductor interfaces can be formed on Si by different technique to passivate interfacial-contamination arisen from the active dangling bonds at the semiconductor surface.

In the present study, Au/$Bi_4Ti_3O_{12}$/n-Si (MFS) structures have been fabricated, and dielectric characteristics of the MFS structures have been investigated in detail both temperature and frequency dependent.

2. EXPERIMENTAL DETAIL

N-type Si substrate was degreased in organic solvent of $CHClCCl_2$, CH_3COCH and CH_3OH consecutively and then etched in a sequence of H_2SO_4 an H_2O_2, 20% HF, a solution of $6HNO_3$: 1 HF: 35 H_2O, 20% HF and finally quenched in de-ionised water for a prolonged time. Preceding each cleaning step, the substrate was rinsed thoroughly in de-ionized water of resistivity of 18 MΩ-cm. After, the Si wafer was mounted on the stainless steel optically heated sputtering holder and loaded in radio frequency (RF) magnetron sputtering system. Then, the Bismuth titanate ($Bi_4Ti_3O_{12}$) was deposited on n-Si with RF magnetron sputtering by using a hot compacting of $Bi_4Ti_3O_{12}$ powder of a stochiometric composition as a target material. The mixture of argon (Ar) and oxygen (O_2) was used a working medium and the substrate was kept at 700 ^{o}C.

For electrical measurements, the pure Au (99.999 %) circular dots with a thickness of about ~2000 Å with a diameter of 1 mm were deposited by a metal evaporation system through a shadow mask on the BTO films. In this way, Au/$Bi_4Ti_3O_{12}$/n-Si (MFS) structures were fabricated on the Si substrate. The structure was mounted on a copper holder with the help of silver paste and the electrical contacts were made to the upper electrodes by the use of tiny silver coated wires with silver paste. The thicknesses of the deposited BTO thin film were found to be about 1000 Å from measurement of capacitance in the strong accumulation region for MFS structure.

The capacitance-voltage (C-V) and conductance-voltage (G/ω-V) measurements were carried out in the wide temperature range of 100-400 K at ten different frequencies (1, 2, 5, 10, 20, 50, 100, 200, 500 and 1000 kHz) by using a HP 4192A LF impedance analyzer and a small ac test signal 50 mV_{rms} from the external pulse generator was applied to the sample in order to meet the requirement. All measurements were controlled by Janes vpf-475 cryostat, which enables us to make measurements in the temperature range of 77-450 K. The sample temperature was always monitored by using a copper-constantan thermocouple close to the sample and by measuring with a dmm/scanner Keithley model 199 and a Lake Shore model 321 auto-tuning temperature controllers with sensitivity better than ±0.1 K.

3. RESULTS AND DISCUSSION

3.1. Frequency and temperature dependence of C and G/ω

Admittance spectroscopy is one of the most popular electrical techniques used to characterize Schottky type devices, i.e. capacitance (C) and conductance (G) at various frequencies as a function of temperature [12]. This technique proved its effectiveness in determination of defect parameters for many semiconductor systems. In order to minimize the effects of dc leakage currents, the measurements were performed at zero voltage at the metal electrode. There has been wide interest in the admittance spectroscopy method for semiconductor investigation, which allows one to obtain information about the parameters of interface. The reason of the existence of the localized electronic states associated with the surface region is the interruption of the periodic lattice structure at the surface, surface preparation, formation of interfacial layer and impurity concentration of semiconductor [22,23]. The admittance (Y) is given by

$$Y(\omega) = G(\omega) + j\omega C(\omega) \tag{1}$$

where G is the conductance, C the capacitance, j the imaginary unit, and ω(=2πf) is the angular frequency.

Figs. 1(a) and (b) show the variation of the C and G/ω as a function of the temperature, measured on an MFS structure, for different values of frequency and at the forward bias of 2.5 V. As shown in Figs. 1(a) and (b), the C and G/ω values are almost constant at low temperatures (T<220 K) and then have displayed an increasing with the increasing temperature. The increase in capacitance and conductance towards high temperature may be due to interfacial space charge formation and increase in thermal activation of charges [22-25]. As expected, the C and G/ω were also greatly enhanced by increasing the temperature, changing by more than one order of magnitude in the temperature range 100-400 K, indicating strongly thermally activated charge carrier mobility.

In addition, the C and G/ω decrease with the increasing frequency. The frequency dependence of the

capacitance and conductance indicate the existence of interface states (N_{ss}) at metal-semiconductor interface. The presence of some interface traps responds to all the frequencies, so the interface state capacitance changes with the frequency. As the frequency is increased, the capacitance decreases to the same limit, as the charges on the defects no longer have time to rearrange in response to the applied voltage [26-28]. Furthermore, at low frequencies, the N_{ss} can easily follow the ac signal and yield an excess capacitance and conductance, which depends on the frequency and time constant of interface states. However, in the sufficiently high frequency limit (f ≥500 kHz), the N_{ss} can hardly follow the ac signal and the contribution of interface states capacitance to the total capacitance can be neglected [11,22,29].

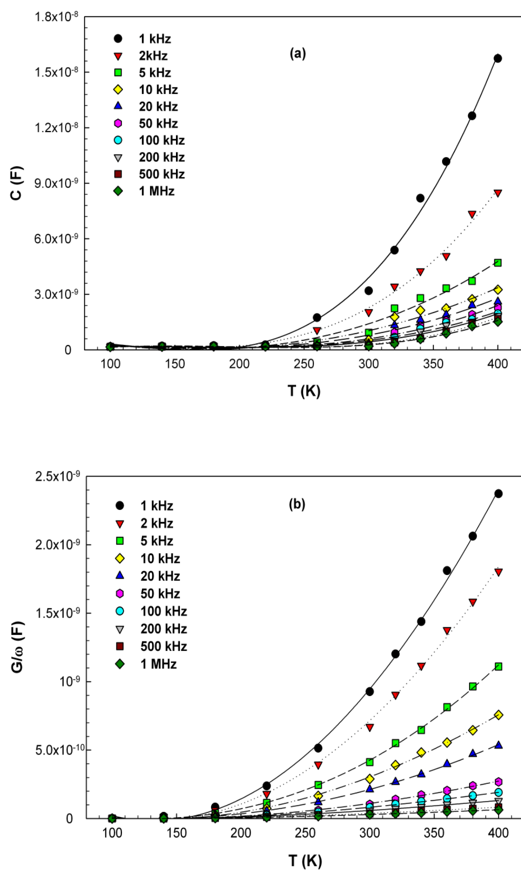

Figure 1. Temperature dependence of (a) capacitance (C) and (b) conductance (G/ω) for an MFS structure at different frequencies and for a dc bias of 2.5 V.

3.2. Frequency and temperature dependence of dielectric permittivity

The complex dielectric permittivity (ε^*) formalism has been employed to describe the electrical and dielectric properties. In the ε^* formalism, in the case of admittance measurements, the following relation holds [30],

$$\varepsilon^* = \frac{Y^*}{j\omega C_o} = \frac{C}{C_o} - j\frac{G}{\omega C_o} \quad (2)$$

where C_o is capacitance of an empty structure such that $C_o = \varepsilon_o(A/d)$; where A is the rectifier contact area in cm^2, d is the oxide layer thickness and ε_0 is the permittivity of free space charge ($\varepsilon_o = 8.85\times10^{-14}$ F/cm).

It is known that the ε^* can be split into a real part (ε') and an imaginary part ε'', according to the equation

$$\varepsilon^*(\omega) = \varepsilon'(\omega) - j\varepsilon''(\omega) \quad (3)$$

Physically, ε' and ε'' represent the charging and the loss current, respectively [31,32]. Moreover, both are frequency and temperature dependent. The real part of the permittivity, $\varepsilon'(\omega)$, is a measure of the energy stored from the applied electric field in the material and identifies the strength of alignment of dipoles in the dielectric. The imaginary part of the permittivity, $\varepsilon''(\omega)$, or loss factor, is the energy dissipated in the dielectric associated with the frictional dampening that prevent displacements of bound charge from remaining in phase with the field changes [33].

The real part of the complex dielectric permittivity, the dielectric constant (ε'), of the MOS structure was calculated using the relation [34,35]

$$\varepsilon' = \frac{C_m}{C_o} \quad (4)$$

where C_m is the measured value of capacitance in the strong accumulation region, corresponding to the oxide capacitance.

On the other hand, the imaginary part of the complex dielectric permittivity, the dielectric loss (ε''), was calculated using the measured conductance (G_m/ω) values from the relation

$$\varepsilon'' = \frac{G_m}{\omega C_o} \quad (5)$$

The dissipation factor or loss tangent (tanδ) can be expressed as follows [34-36],

$$\tan\delta = \frac{\varepsilon''}{\varepsilon'} \quad (6)$$

Figs. 2(a) and (b) show the temperature dependence of the real part (ε') and imaginary (ε'') of dielectric permittivity ($\varepsilon^* = \varepsilon' - j\varepsilon''$) as a function of temperature (100-400 K) for ten frequency values, respectively. As shown in Figs. 2(a) and (b), the values of the dielectric constant (ε') and dielectric loss (ε'') is almost temperature independent in the interval 100-220 K, while increase with the increasing temperature in the interval 220-400 K. As the temperature rises,

imperfections/disorders are created in the lattice and the mobility of the majority charge carriers (ions and electrons) increases. The values of ε' and ε'' increase with an increase in temperature which can be attributed to the fact that the orientation polarization is connected with the thermal motion of molecules, so dipoles can not orient themselves at low temperatures [22]. When the temperature is increased the orientation of dipoles is facilitated and this increases the value of orientational polarization, which increases ε' and ε'' [11,18,28,31,32,37-39].

Furthermore, the frequency dependences of the ε' and ε'' are probably related to the presence of an interfacial surface, at the electrode-film interface, which results in an undesirable Maxwell-Wagner-type dispersion in the dielectric data. The decrease in ε' and ε'' with the increasing frequency is explained by the fact that as the frequency is raised, the interfacial dipoles have less time to orient themselves in the direction of the alternating field. As the frequency increases, charges can no longer follow the field and their contribution to the dielectric constant ceases [27,36,37,40-42].

Fig. 2(c) shows the variation of dielectric loss tangent (tanδ) with temperature at various frequencies. As shown in Fig. 2(c), the value of tanδ increases with the increasing temperature in the interval 100-300 K, while it decreases and is almost temperature independent in the interval 300-400 K. Also, the tanδ decreases with the increasing frequency at all temperatures. If the electric polarization in a dielectric is unable to follow the varying electric field, dielectric loss occurs. An applied field will alter this energy difference thus producing a net polarization. This part of the polarization, which is not in phase with the applied field, is termed as dielectric loss [38].

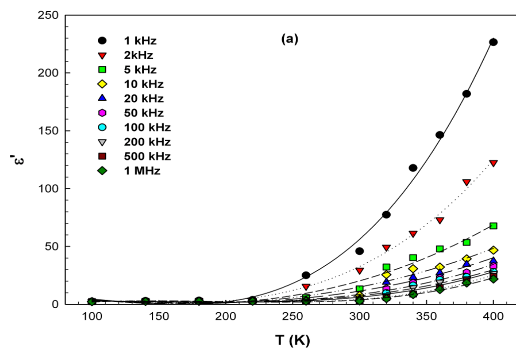

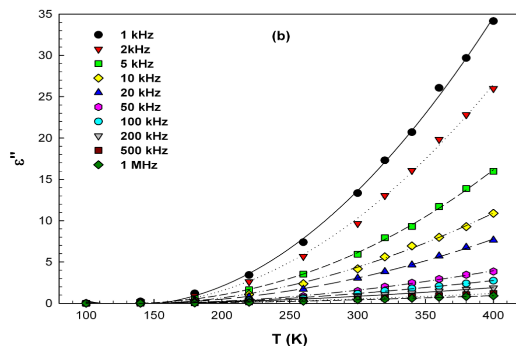

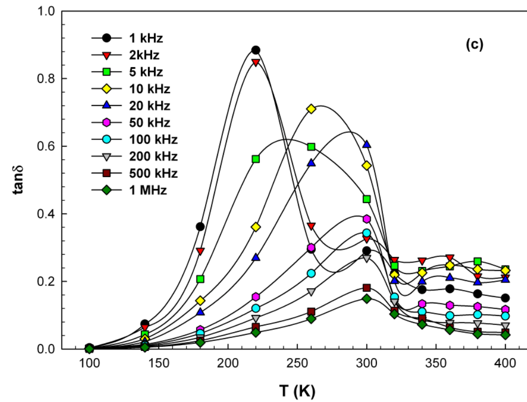

Figure 2. Temperature dependence of (a) ε', (b) ε'' and (c) tanδ of MFS structure at various frequencies.

3.3. AC conductivity

The frequency-dependent ac conductivity (σ_{ac}) is obtained from the dielectric losses according to the relation [28,43-45]

$$\sigma^* = j\varepsilon_0\omega\varepsilon^* = j\varepsilon_0\omega(\varepsilon' - j\varepsilon'') = \varepsilon_0\omega\varepsilon'' + j\varepsilon_0\omega\varepsilon' \tag{7}$$

The real part of complex conductivity (σ^*) is calculated using the relation

$$\sigma_{ac} = \omega\varepsilon_o\varepsilon' \tan\delta = \varepsilon_0\omega\varepsilon'' \tag{8}$$

Fig. 3 illustrates the temperature dependence of ac conductivity (σ_{ac}) of MFS structure at different values of frequencies. The σ_{ac} shows an increasing trend with the increasing frequency and temperature. The increase in the σ_{ac} with the increasing temperature can be attributed to the impurities or dislocations at metal-semiconductor interface. These impurities lie below the bottom of the conduction band and thus it has small activation energy [36,37,42-45]. The frequency dependence of conductivity in the relaxation phenomenon arises due to mobile charge carriers. For a region of frequencies where the conductivity increases strongly with frequency, the transport is dominated by contributions from hopping of charge carriers among the trap levels situated in the band gap [27,28,31,32,39,45-47].

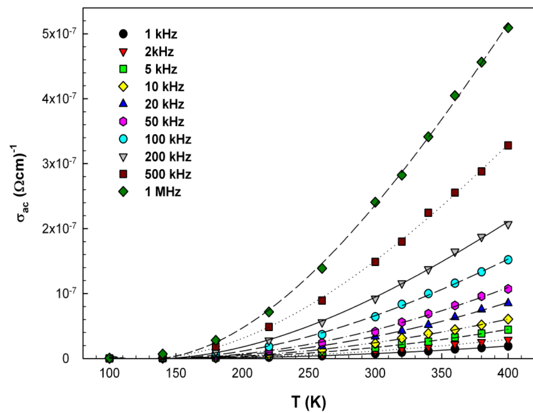

Figure 3. Variation of ac conductivity (σ_{ac}) with temperature at different frequencies.

The ac conductivity (σ_{ac}) is related to the activation energy and the inverse absolute temperature, using an empirical relation:

$$\sigma_{ac} = \sigma_o e^{(-E_a/k_B T)} \quad (9)$$

where σ_o is the composite constant or the pre-exponential factor, E_a the activation energy of the conduction mechanism, k_B the Boltzmann constant and T is the temperature in Kelvin [28,31,36,37,45,48]. The Arrhenius plots ($\ln\sigma_{ac}$ vs 1000/T) of ac conductivity at different frequencies are shown in Fig. 4. The activation energy, E_a, was calculated from the straight line fitting of plots shown in Fig. 4 and the values are presented in Fig. 5. As shown in Fig. 5, the E_a decreases with the increasing frequency. The E_a values were found to vary from 93.4 to 78.7 meV for MFS structure within the experimental temperature range. The increase in the applied field enhances the charge carrier's jumps between the localized states, consequently, the activation energy decreases with the increasing frequency. Also, the obtained low values of activation energy suggests that the conduction mechanism may be due to the hopping of electrons [44,49,50].

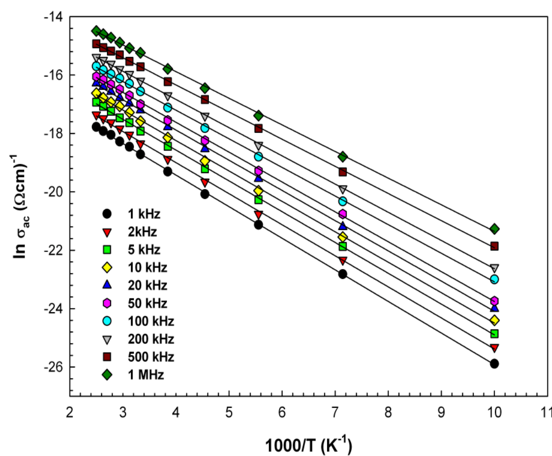

Figure 4. Arrhenius plots of ac conductivity of MFS structure for different frequencies.

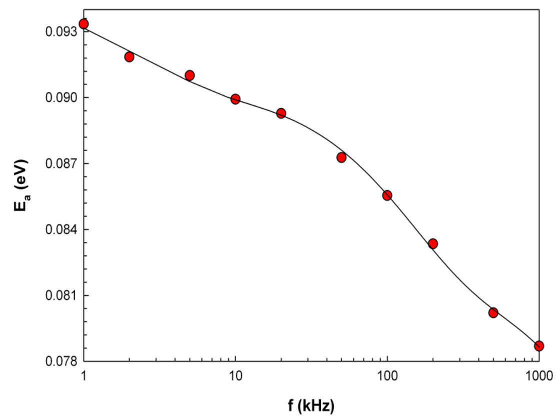

Figure 5. Variation of activation energy (E_a) with frequency.

In addition, a convenient formalism to investigate the frequency behavior of conductivity is based on the power law relation proposed by Jonscher [51],

$$\sigma(\omega) = \sigma_{dc} + \sigma_{ac} = \sigma_{dc} + A\omega^s \quad (10)$$

where $\sigma(\omega)$ is the total conductivity. The first term is the temperature-dependent (frequency-independent) dc conductivity and is related to the drift mobility of the electric charge carriers. The second term represents the frequency and temperature dependent ac conductivity (σ_{ac}) and is attributed to the dielectric relaxation caused by the localized electric charge carriers. A is a temperature-dependent constant and s is the power law frequency exponent which generally varies between 0 and 1. Moreover, the dependence of s on temperature is a function of conduction mechanism [32,37,40,45,52,53].

Fig. 6 shows the ln σ_{ac} vs. ln f plots of frequency-dependent ac conductivity of MFS structure at various temperatures. The σ_{ac} increases with the increasing frequency and temperature. Fig. 7 displays the temperature dependence of frequency exponent, s, for MFS structure. The value of s for each temperature was determined from the slopes of ln σ_{ac} vs. ln f plots (Fig. 6). It is observed that the s decreases with the increasing temperature. The s values were found to vary from 0.64 to 0.45 within the experimental temperature range. The temperature-dependent parameter s represents the extent of interactions among charge carriers and defect states.

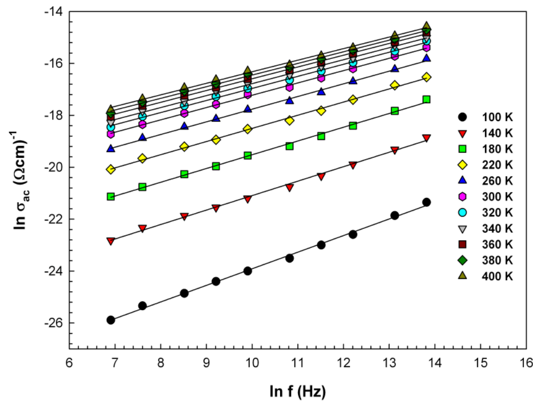

Figure 6. Frequency dependence of the ac conductivity of MFS structure at different temperatures.

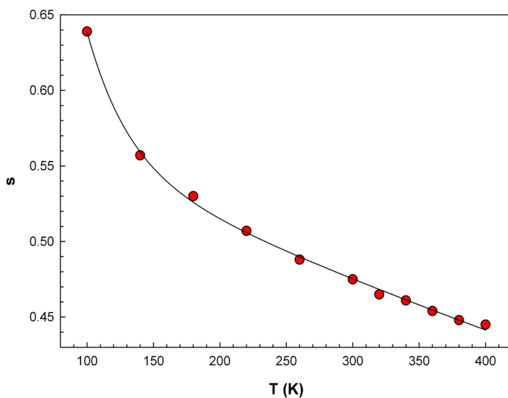

Figure 7. Temperature variation of the frequency exponent of MFS structure.

3.4. Electric modulus

Electrical transport process parameters (such as carrier/ion hopping rate; conductivity relaxation time, etc.) in the material can be analyzed via complex electric modulus formalism. The electric modulus M^* as expressed in the complex modulus formulism [31,52-55]:

$$M^* = \frac{1}{\varepsilon^*} = M' + jM'' \tag{11}$$

The real part (M') and the imaginary part (M'') of the complex electric modulus (M^*) can be expressed as

$$M' = \frac{\varepsilon'}{(\varepsilon')^2 + (\varepsilon'')^2} \quad \text{and}$$

$$M'' = \frac{\varepsilon''}{(\varepsilon')^2 + (\varepsilon'')^2} \tag{12}$$

The real component M' and the imaginary component M'' were calculated from ε' and ε''. The temperature dependence of the real (M') and imaginary part (M'') of complex modulus (M^*) for various frequencies is shown in Figs. 8(a) and (b) for MFS structure. As seen in Fig. 8(a), the M' decreases with the increasing temperature. As frequency increases, the value of M' increases and reaches almost a constant value at higher temperatures. The imaginary part of electrical modulus is indicative of energy loss in the structure under electrical field. As shown in Fig. 8(b), the M'' gives a peak at temperatures lower than about 300 K for all frequencies. The position of the peaks shifts to higher temperature with the increasing frequency. The region where peak occurs is indicative of the transition from long range to short-range mobility with increase in frequency. This type of behavior of the modulus spectrum is suggestive of temperature dependent hopping type mechanism for electrical conduction (charge transport) in the system [28,40,42,45,50-57].

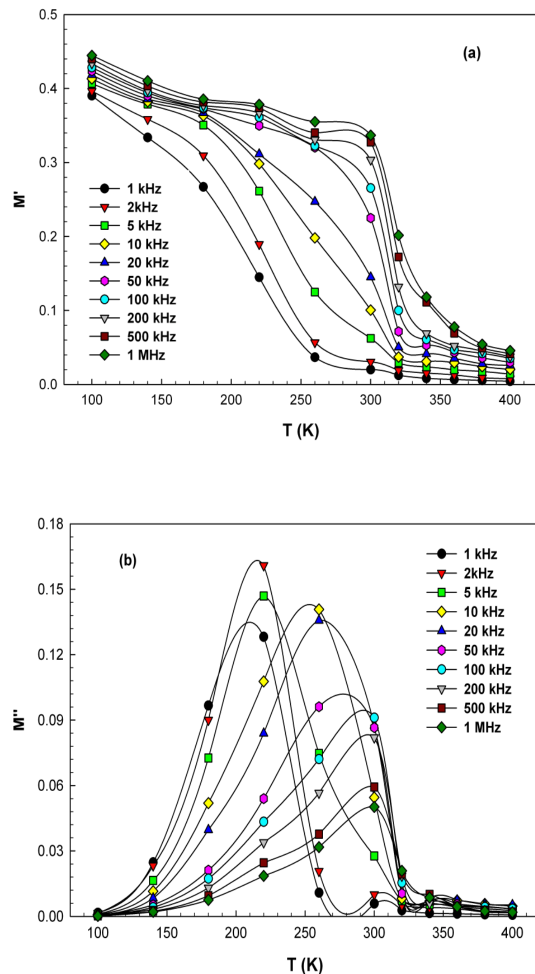

Figure 8. Temperature dependence of (a) real part M' and (b) imaginary part M'' of electric modulus M^* at various frequencies.

4. CONCLUSIONS

The temperature and frequency dependence of the dielectric permittivity, conductivity and modulus of $Au/Bi_4Ti_3O_{12}/n\text{-}Si$ (MFS) structure have been investigated. The experimental results show that the values of ε' and ε'' are found to decrease with the increasing frequency and increase with the increasing temperature. The frequency and temperature dependence of ε' is attributed to interfacial and

orientational polarization, whereas the frequency and temperature dependence of ε'' is associated with the conduction loss. The value of σ_{ac} increases with the increasing frequency and temperature. The increase in the σ_{ac} with the increasing temperature is attributed to the impurities or dislocations at metal-semiconductor interface. Regarding the small value of activation energy along with the frequency dependence of conductivity, the conduction mechanism was suggested to be hopping conduction. An analysis of the experimental data shows that hopping of charge carriers between localized states is the dominant conduction mechanism, and the physical model, based on classical hopping of electrons over a barrier, predicts a decrease of s with an increase in temperature. The real (M') and imaginary part (M'') of complex modulus (M^*) were calculated from the values of ε' and ε''. The frequency and temperature dependence of C-V and G/ω-V characteristics confirmed that both frequency and temperature strongly affect the dielectric permittivity, ac conductivity and electric modulus.

REFERENCES

[1] N.V. Giridharan, R. Varatharajan, R. Jayavel, P. Ramasamy, ***Mater. Chem. Phys***. 65 (2000) 261

[2] A. Mansingh, ***Ferroelectrics*** 102 (1990) 69.

[3] N. Kumari, J. Parui, K.B.R. Varma, S.B. Krupanidhi, ***Solid State Comm***. 137 (2006) 566.

[4] T.A. Rost, H. Lin, T.A. Rabson, ***Appl. Phys. Lett***. 59 (1991) 3654.

[5] Zh. Wang, Ch.H. Yang, X.Y. Yu, T. Yu, ***J. Crys. Growth*** 280 (2005) 557.

[6] T. Hirai, K. Teramoto, K. Nagashima***, Jpn. J. Appl. Phys.*** 34 (1995) 4163.

[7] J.J. Zhang, J. Sun, X.J. Zheng, ***Solid-State Electron.*** 53 (2009) 170.

[8] V.R. Palkar, S.C. Purandare, R. Pinto, ***J. Phys. D: Appl. Phys.*** 32 (1999) R1.

[9] E. Rokuta, Y. Hotta, T. Kubota, H. Tabata, H. Kobayashi, T. Kawaia, ***Appl. Phys. Lett.*** 79 (2001) 403.

[10] K. Aizawa, E. Tokumitsu, K. Okamoto, H. Ishawara, ***Appl. Phys. Lett.,*** 7 (2000) 2609.

[11] F. Parlaktürk, Ş. Altındal, A. Tataroğlu, M. Parlak, A. Agasiev, ***Microelectron. Eng***. 85 (2008) 81.

[12] C.K. Lee, W.S. Kim, H. Park, H. Jeon, Y.H. Pae, ***Thin Solid Films*** 473 (2005) 335.

[13] A. Fouskova, L.E. Cross, ***J. Appl. Phys***. 41 (1970) 2834.

[14] L.B. Kong, J. Ma, ***Thin Solid Films*** 379 (2000) 89.

[15] S.Y. Wu, ***J. Appl. Phys***. 50 (1979) 4314.

[16] D. Wu, A. Li, N. Ming, ***Microelectron. Eng***. 66 (2003) 773.

[17] J.P. Han, T.P. Ma, ***Appl. Phys. Lett***. 72 (1998) 1185.

[18] P.C. Joshi, S.B. Desu, ***J. Appl. Phys***. 80 (1996) 2349.

[19] E.B. Araujo, J.A. Eiras, ***J. Phys. D: Appl. Phys***. 32 (1999) 957.

[20] W.L. Liu, H.R. Xia, H. Han, X.Q. Wang***, J. Crys. Growth*** 264 (2004) 351.

[21] Ş. Altındal, F. Parlaktürk, A. Tataroğlu, M.M. Bülbül, ***J. Optoelectron. Adv. Mater***. 12 (2010) 2139.

[22] E.H. Nicollian, J.R. Brews, Metal oxide semiconductor (MOS) physics and technology, ***John Willey & Sons***, New York, 1982.

[23] E.H. Nicollian and A. Goetzberger, ***Appl. Phys. Lett.*** 7 (1965) 216.

[24] M.D. Kannan, S.K. Narayandass, C. Balasubramanian, D. Mangalaraj, ***Phys. Stat. Sol.*** (a) 121 (1990) 515.

[25] Zh. Wang, Ch.H. Yang, X.Y. Yu, T. Yu, ***J. Crys. Growth*** 280 (2005) 557.

[26] L. Fu, K. Liu, B. Zhang, J. Chu, ***Appl. Phys. Lett.*** 72 (1998) 1784.

[27] P. Matheswaran, R. Sathyamoorthy, R. Saravanakumar, S. Velumani, ***Mater. Sci. Eng. B*** 174 (2010) 269.

[28] K. Prabakar, S.K. Narayandass, D. Mangalaraj, ***Phys. Stat. Sol***. (a) 199 (2003) 507.

[29] J.H. Werner, Metallization and Metal-Semiconductor Interface, ***Plenum***, New York, 1989.

[30] N.G. McCrum, B.E. Read, G. Williams, Anelastic and Dielectric Effects in Polymeric Solids, ***Wiley***, New York, 1967.

[31] A. Eroğlu, A. Tataroğlu, Ş. Altındal, ***Microelectron. Eng***. 91 (2012) 154.

[32] M.M. Abdel Kader, M.Y. Elzayat, T.R. Hammad, A.I. Aboud, H. Abdelmonem, ***Phys. Scr***. 83 (2011) 035705.

[33] D. Cheng, Field and Wave Electromagnetics, 2nd Ed., ***Addison-Wesley***, New York, 1989.

[34] A. Chelkowski, Dielectric Physics, ***Elsevier,*** Amsterdam, 1980.

[35] M. Popescu, I. Bunget, Physics of Solid Dielectrics, ***Elsevier***, Amsterdam, 1984.

[36] A. Tataroğlu, ***J. Optoelectron. Adv. Mater***. 13 (2011) 940.

[37] S. Maity, D. Bhattacharya, S.K. Ray, ***J. Phys. D: Appl. Phys***. 44 (2011) 095403.

[38] L. Kungumadevi, R. Sathyamoorthy, A. Subbarayan, ***Solid-State Electron***. 54 (2010) 58.

[39] J.S. Kim, H.J. Lee, S.Y. Lee, I.W. Kim, S.D. Lee, Thin Solid Films 518 (2010) 6390.

[40] N. Singh, A. Agarwal, S. Sanghi, ***Current Appl. Phys***. 11 (2011) 783.

[41] E.B. Araújo, J.A. Eiras, ***J. Phys. D: Appl. Phys***. 32 (1999) 957.

[42] A.K. Dubey, P. Singh, S. Singh, D. Kumar, O. Parkash, ***J. Alloys Compd***. 509 (2011) 3899.

[43] M.A. Elkestawy, S. Abdel kader, M.A. Amer, ***Physica B*** 405 (2010) 619.

[44] A.M. Farid, H.E. Atyia, N.A. Hegab, ***Vacuum*** 80 (2005) 284.

[45] A.A.M. Farag, A.M. Mansour, A.H. Ammar, M. Abdel Rafea, A.M. Farid, ***J.Alloys Compd***. 513 (2012) 404.

[46] K.C. Verma, M. Ram, J. Singh, R.K. Kotnala, ***J. Alloys Compd***. 509 (2011) 4967.

[47] L. Agrawal, A. Dutta, S. Shannigrahi, B.P. Singh, T.P. Sinha, ***Physica B*** 406 (2011)

[48] M.P. Kumar, T. Sankarappa, G.B. Devidas, P.J. Sadashivaiah, ***Mater. Sci. Eng***. 2 (2009) 012050.

[49] B. Louati, F. Hlel, K. Guidara, ***J. Alloys Compd***. 486 (2009) 299.

[50] ,.A. Hegab, M.A. Afifi, H.E. Atyia, A.S. Farid, ***J. Alloys Compd.*** 477 (2009) 925.

[51] A.K. Jonscher, Universal Relaxation Law, ***Chelsea Dielectric Press***, London, 1996.

[52] F. Yakuphanoğlu, ***Physica B*** 393 (2007) 139.

[53] T.Z. Rizvi, A. Shakoor, ***J. Phys. D: Appl. Phys***. 42 (2009) 095415.

[54] Moti Ram, S. Chakrabarti, ***J. Alloys Compd***. 462 (2008) 214.

[55] R. Ertuğrul, A. Tataroğlu, ***Chin. Phys. Lett***. 29(7) (2012) 077304.

[56] I.S. Yahia, M.S. Abd El-sadek, F. Yakuphanoğlu, ***Dyes and Pigments*** 93 (2012) 1434.

[57] M.B. Mohamed, H. Wang, H. Fuess, ***J. Phys. D: Appl. Phys.*** 43 (2010) 455409.